frontiers | Frontiers in Sensors

TYPE Original Research
PUBLISHED 22 November 2022
DOI 10.3389/fsens.2022.1066974

Check for updates

OPEN ACCESS

EDITED BY
Chang-Soo Lee,
Chungnam National University, South Korea

REVIEWED BY
Nae Yoon Lee,
Gachon University, South Korea
Heon-Ho Jeong,
Chonnam National University, South Korea

*CORRESPONDENCE
Yong Kyoung Yoo,
yongkyoung0108@cku.ac.kr
Jeong Hoon Lee,
jhlee@kw.ac.kr

SPECIALTY SECTION
This article was submitted to Lab-on-a-Chip Devices, a section of the journal Frontiers in Sensors

RECEIVED 11 October 2022
ACCEPTED 07 November 2022
PUBLISHED 22 November 2022

CITATION
Lee S, Kim J, Lee NE, Kim KH, Park SJ, Park JS, Kim C, Hong JH, Yoon DS, Yoo YK and Lee JH (2022), Three-dimensional ready-to-pick reservoir-based preconcentrator with a pillar-structured channel for miRNA applications.
Front. Sens. 3:1066974.
doi: 10.3389/fsens.2022.1066974

COPYRIGHT
© 2022 Lee, Kim, Lee, Kim, Park, Park, Kim, Hong, Yoon, Yoo and Lee. This is an open-access article distributed under the terms of the Creative Commons Attribution License (CC BY). The use, distribution or reproduction in other forums is permitted, provided the original author(s) and the copyright owner(s) are credited and that the original publication in this journal is cited, in accordance with accepted academic practice. No use, distribution or reproduction is permitted which does not comply with these terms.

Three-dimensional ready-to-pick reservoir-based preconcentrator with a pillar-structured channel for miRNA applications

Seungmin Lee[1,2], Jinhwan Kim[1], Na Eun Lee[1,3], Kang Hyeon Kim[1], Seong Jun Park[1], Jeong Soo Park[1], Cheonjung Kim[1,4], Ji Hye Hong[1,2], Dae Sung Yoon[2], Yong Kyoung Yoo[4]* and Jeong Hoon Lee[1]*

[1]Department of Electrical Engineering, Kwangwoon University, Seoul, South Korea, [2]School of Biomedical Engineering, Korea University, Seoul, South Korea, [3]Department of Biotechnology, College of Life Sciences and Biotechnology, Korea University, Seoul, South Korea, [4]Department of Electronic Engineering, Catholic Kwandong University, Gangneung-si, South Korea

A sample preconcentration technique that exceeds a microfluidic device's limited processing volume (up to microliters) is critical for real sample pretreatment applications. Here, we have developed a 3D-printed preconcentrator with a pillar structure (3DP^2) to enrich the biological samples up to hundreds of microliter scales (700 µL) within 20 min by utilizing ion concentration polarization (ICP). We designed three-dimensional ready-to-pick reservoirs serially connected with a pillar-structured channel to enable large-volume preconcentration by balancing the preconcentrating forces (depletion, electrophoretic, and electroosmotic force) generated by ICP. Using the I-t and I-V curves, we confirmed that ICP performance was enhanced due to a pillar structure's suppression of the vortex. Finally, we preconcentrated bovine serum albumin (BSA) and micro ribonucleic acid-21 (miRNA-21) two-fold. Moreover, depending on their size and charge, these were concentrated at different locations and could be extracted easily using pipettes. We believe that this study provides a novel strategy for downstream applications.

KEYWORDS

ion concentration polarization, MiRNA-21, 3D printing, preconcentration, electrokinectic

Introduction

Many biomarkers regarding health status exist in the body fluids, including nucleic acids, proteins, enzymes, antibodies, vesicles, and cells (Bertrand et al., 2014; O'Connor et al., 2017; Hindson et al., 2013). In diagnostics, these biomarkers are used for early detection, disease prognosis, and therapeutic development (Tivey et al., 2022; Heitzer et al., 2019; Heikenfeld et al., 2019; Wang et al., 2016) (Wang et al., 2016; Heikenfeld et al., 2019; Heitzer et al., 2019; Tivey et al., 2022). For example, different types of microRNAs (miRNAs) contained in human blood or exosomes are promising cancer biomarkers, and certain groups of miRNAs are strongly related to the expression of specific cancer (Heikenfeld et al., 2019; Wang et al., 2016; Sajid et al., 2016; Purwidyantri et al., 2021) (Sajid et al., 2016; Wang et al., 2016; Heikenfeld et al., 2019; Purwidyantri et al., 2021). Despite of tremendous potential of biomarkers, these only exist at very low concentrations in the body fluids; the total concentration of miRNA extracted from human plasma is 1.1–6.2 pg/ml, and it is even lower in other biofluids such as spinal fluid and urine (Brennan et al., 2020; Chen et al., 2021) (Brennan et al., 2020; Chen et al., 2021a). Moreover, inhibitors coexist with the target biomarker, hampering biomarker detections in molecular diagnostics and immunoassays (Sajid et al., 2016; Purwidyantri et al., 2021) (Sajid et al., 2016; Purwidyantri et al., 2021). Diagnostic tools and methods using nucleic acid detection suffer from the above reasons. Therefore, selective sample enrichments and inhibitor removal functions are essential for miRNA sample preparations.

To realize the preconcentration with separating functions, ultra-centrifugation (Brennan et al., 2020; Chen et al., 2021; Nguyen et al., 2021) (Brennan et al., 2020; Chen et al., 2021a; Nguyen et al., 2021) and filtration (Fan et al., 2019; Cao et al., 2021; Alele et al., 2016) (Alele and Ulbricht, 2016; Fan et al., 2019; Cao et al., 2021) are considered the golden standard. The ultra-centrifugation method separates biomolecules based on their density; it can greatly assist in improving the performance of detecting nucleic acid in body fluids. However, it is expensive and requires adequate expertise, analysis time, and equipment. Alternately, the filtration method separates biomolecules based on their size. However, several limitations exist, such as low yield, low selectivity, and slow filtration speed. Furthermore, the sample can be easily lost and damaged with the process due to applied shear stress and non-specific binding to the filter. Highly efficient and selective preconcentration techniques with easy operation applied to analytical methods are needed to detect the low concentration sample.

To overcome hurdles of ultra-centrifugation and filtration methods, ion concentration polarization (ICP) preconcentration is considered a great candidate since ICP can quickly concentrate and separate the charged particle with simple electric operation without any chemical (Park et al., 2016; Li et al., 2016; Kim et al., 2013) (Kim et al., 2013; Li and Anand, 2016a; Park et al., 2016). Due to the applied electric field in microfluidics, charged ions are moved toward the oppositely charged electrode through an ion-permselective membrane. As a result, a depletion zone is formed, and charged biomolecules are accumulated in the enrichment zone. Most ICP-based preconcentrators have been demonstrated on a microfluidic platform, where the channel larger than millimeter-scale causes severe turbulence (vortex), making ICP unstable (Morini et al., 2004; Kandlikar et al., 2008) (Morini et al., 2004; Kandlikar and Li, 2008). These ICP preconcentrators in polydimethylsiloxane (PDMS)-based microfluidic channel has several problems, such as small processing volume, needs of mold for fabrication, and the difficulty of applying to other applications. To address these problems, we previously reported ICP preconcentration in a cellulose paper chip with microfluidics to address the limitations (Lee et al., 2021; Han et al., 2016) (Han et al., 2016; Lee et al., 2021). Cellulose fiber networks in the paper chip served as multi-microchannel, enabling the ICP preconcentration to be more stable, then providing stable preconcentration without significant turbulence (Deng et al., 2013; Anna et al., 2014) (Deng et al., 2013; Anna et al., 2014). We reported a microfluidic paper-based large-volume preconcentrator to enrich and separate biomarkers simultaneously (Lee et al., 2021; Kim et al., 2022) (Lee et al., 2021; Kim et al., 2022). However, the paper-based ICP preconcentration has critical issues to overcome. For example, we needed an extra extraction step, such as centrifugation or squeezing, when we used paper materials for ICP operation to apply other analytical methods. In addition, it needs additional surface treatment to prevent the adsorption and losses of collected samples. There has been an attempt to fabricate microfluidic devices using 3D printing (Razavi Bazaz, S. et al., 2020; Prabhakar, P. et al., 2021) (Razavi Bazaz et al., 2020; Prabhakar et al., 2021). With the assistance of 3D printing, the microfluidic device can easily be fabricated (up to a micrometer scale) without any mold, and surface characteristics can be controlled by using various commercial resins without any surface treatment.

In this study, we developed a 3D-printed preconcentrator with a pillar-structured channel ($3DP^2$) for selective sample preconcentration and separation in large-capacity bio-samples. We designed three-dimensional ready-to-pick reservoirs serially connected with a pillar-structured channel for biomarker enrichment with separation function (Figure 1). We fabricated $3DP^2$ using a 3D printer. Nafion membranes are located with both side of the reservoirs to apply ICP phenomena. With the ICP preconcentration, we could easily extract the enrichment samples by pipetting. To realize the stable preconcentrator, we designed the pillar structure in the connecting channel between the reservoirs, reducing the vortex by placing the pillar structure in channels (Kim et al., 2017) (Kim et al., 2017a). After demonstrating the electrical characteristics of ICP with I-t and I-V curves, we tested the ability of reservoir-type ICP preconcentration with a spectrophotometer and successfully

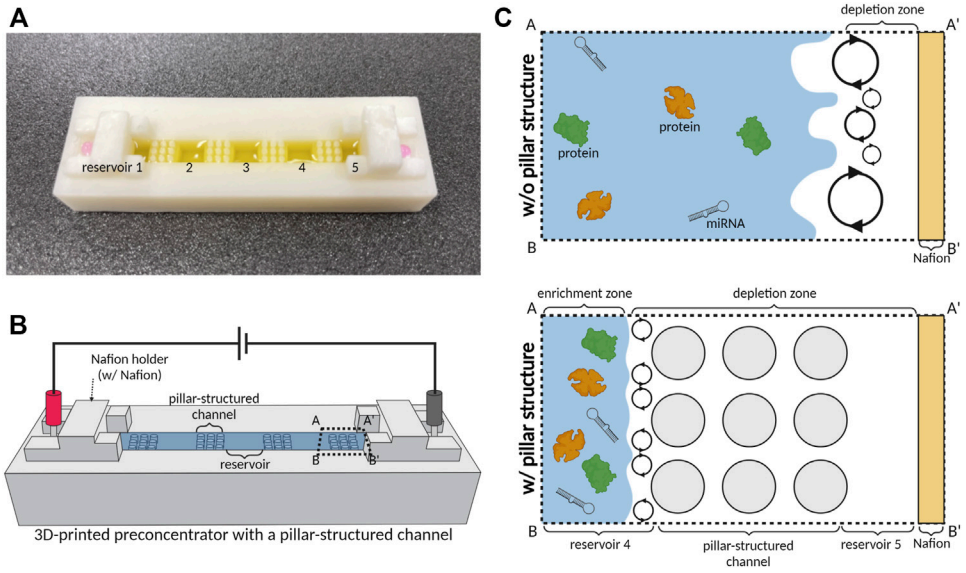

FIGURE 1
Schematic illustration of a 3D-printed preconcentrator with a pillar-structured channel (3DP^2). **(A)** Optical image of a 3D-printed device with five reservoirs connected with a pillar-structured channel. **(B)** Scheme showing the preconcentration of 3DP^2. **(C)** Schematic diagrams of preconcentration with pillar structure. We applied the electrical field of 100 V across millimeter-scale channels and reservoirs and acquired the stable preconcentration only with a pillar-structured channel between reservoirs.

enriched bovine serum albumin (BSA) and miRNA-21 with enhanced stability.

Material and method

Device fabrication

We first designed a 3D-printed preconcentrator with five reservoirs and serially connected channels using Rhinoceros 3D software (Robert McNeel and Associates, United States). Then, to show the pillar structure effects, we prepared two designs; the first design is the pillared channel structures, and the second is prepared without pillar structure in channels. Next, we designed 3 × 3 arrays with a diameter of 2 mm with 2 mm offsets. To fabricate a 3D-printed preconcentrator, we imported the designed model onto a 3D printer through the Z-SUITE program (Zortrax, Poland). Then, using commercial resin (Formlabs, United States), we printed the preconcentrator using the 3D printer Inkspire (Zortrax, Poland), as shown in Figure 1A. Resin is cured with the 405 nm wavelength (Power: 75 W) and exposed to light within 9.5 s for each layer. The thickness of the layer is 0.05 mm. In Figure 1B, we attached the Nafion permselective membrane to the reservoirs on the cathodic and anodic sides to add the permselectivity. For this, we used double adhesive tape (3M, United States) and Nafion 117 (Sigma-Aldrich, United States) and prepared with a dimension of 5 × 12 mm using a cutting machine (Silhouette, United States). Lastly, we punched out a hole double side tape to function reservoirs, then dropped 20 μL of 1 × PBS buffer (Sigma-Aldrich, United States) onto reservoirs. Finally, we applied voltage *via* Pt electrodes. After experiments, devices were washed using ethanol and distilled water for reuse.

Materials and reagents

To visualize the enrichment process, we used the Orange-G dye (Sigma-Aldrich, United States) as a negatively charged color dye. The sample was prepared by diluting the Orange-G to 0.1 mg/ml in 0.1 × PBS. BSA (Sigma-Aldrich, United States) and miRNA-21 (BIONEER, Republic of Korea) were used to evaluate enrichments.

Sample preconcentration and analysis

For sample preconcentration, we injected the sample of 700 μL into 3DP^2 with and without a pillar-structured channel. We applied voltage with a current-voltage source measurement unit (Keithley 2,400, Keithley Instruments, Inc. United States), operated with the LabVIEW program (National Instrument, United States). To acquire current-voltage (I-V) curves and current-time (I-t) measurements, we used the

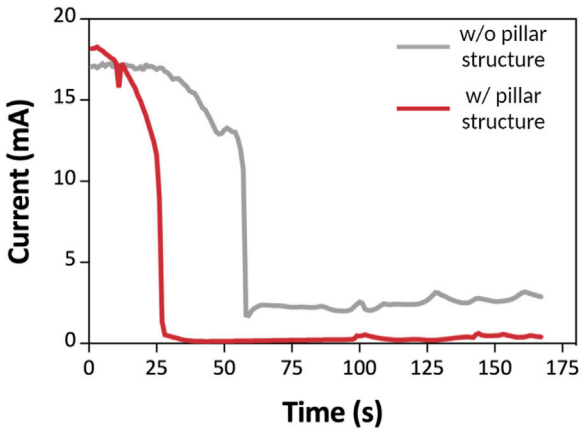

FIGURE 2
I-t curve of 3DP^2 with an applied voltage of 100 V within 170 s. I-t curve of the 3DP^2 without (gray line) and with (red line) a pillar-structured channel. The current decreases according to the propagation of the depletion zone.

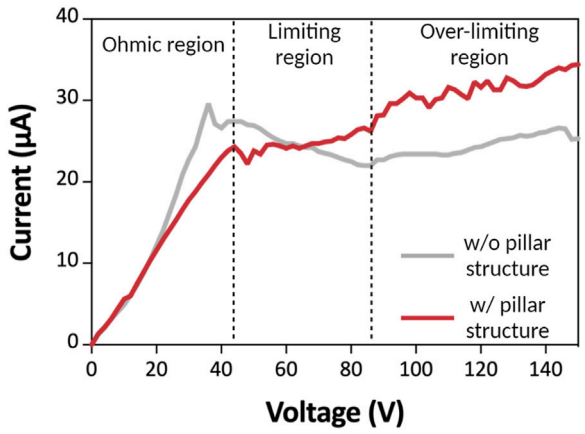

FIGURE 3
Current-voltage curves. I-V curve of the 3DP^2 without (gray line) and with (red line) pillar-structured channel. There are three regions: In the ohmic region, the current increases as the voltage increase in a linear relationship. In limiting regions, the current is maintained at a certain level. At last, in the over-limiting region, the current increases in non-linear form, and the depletion zone propagates.

current-voltage source measurement unit operated with the LabVIEW program. We examined the current voltage and current-time curves to observe the ICP's functions.

We used Nanodrop (Thermo Fisher, United States) as a spectrophotometer. The wavelength of 480 nm was used for fluorescence dye, and 260 nm and 280 nm for miRNA-21 and BSA. For sodium dodecyl sulfate–polyacrylamide gel electrophoresis (SDS-PAGE) analysis, separating gel (Acrylamide 10%, pH 8.8) and stacking gel (Acrylamide 5%, pH 6.8) were prepared for SDS-PAGE gel. Laemmli sample buffer (Bio-Rad Laboratories, Inc. United States) and 2-Mercaptoethanol (Sigma-Aldrich, United States) were added to the sample and boiled at 95℃ for 5 min. The 10 μL of mixtures were loaded into each reservoir of the SDS-PAGE gel. Gels were run at 150 V in running buffer (25 mm Trizma base (Sigma-Aldrich, United States), 250 mm Glycine (Sigma-Aldrich, United States), 3.4 mm SDS (Sigma-Aldrich, United States), pH 8.3) and stained at Coomassie brilliant blue R-250 (Bio-Rad Laboratories, United States) for 10 min. Thereafter, we analyzed gel images using the ImageJ software (Wayne Rasband, National Institute of Health, Bethesda, MD, United States).

Results

Current-time curve of ICP

To observe the formation of the depletion zone, we monitored current changes with time in Figure 2. When we used a millimeter-scale channel under an electric field for operating ICP, the current trend changed with time if ICP was induced (Han et al., 2016; Chen et al., 2021) (Han et al., 2016; Chen et al., 2021b). To confirm the effect of pillar structure on ICP, the current-time curve was observed. When an electric field (100 V) was applied on an ion permselective membrane, such as Nafion, ICP occurred close to the membrane. Subsequently, the cation was depleted on one side of the membrane, while the cation was enriched on the other (Kwak et al., 2016; Li et al., 2016) (Kwak et al., 2016a; Li and Anand, 2016b). In the depleted region, resistance increased due to a lack of ions (Lee et al., 2017; Kim et al., 2017) (Kim et al., 2017b; Lee et al., 2017). Therefore, the resistance increased as the depletion zone of ICP formed. However, when the system had a high Reynolds number, an unstable flow (vortex) was generated, destroying the depletion zone. The vortex transferred ions to the depletion zone, and the current increased. To examine the effect of a pillar-structured channel on ICP phenomenon, we obtained a current-time curve in 0.1×PBS buffer and analyzed the curve's trend (Figure 2) during 170 s. Figure 1C shows that the pillar-structured channel increases the stability of ICP by reducing the Reynolds number. The current drastically dropped and remained near zero with the pillar structure (red line in Figure 2). However, without a pillar structure (gray dot in Figure 2), the current slowly decreased and remained at a higher value than that in the former case. Under an applied voltage of 100 V, we confirmed the stability of ICP with a pillar-structured channels in a millimeter-scale fluidic device.

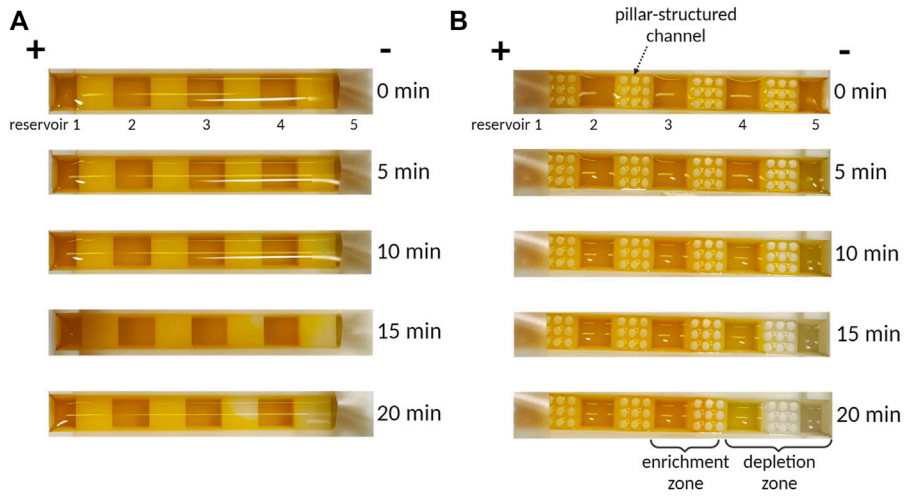

FIGURE 4
The photographs of preconcentration of Orange-G dye according to time. **(A)** Without pillar structure, depletion zone propagation is weak due to unstable vortex flux. **(B)** With a pillar structure, depletion zone propagation is strong to go more than twice that of without pillars.

Current-voltage curve of ICP

We observed the current-voltage response to confirm the profile of the ICP phenomenon of 3DP^2 with and without a pillar-structured channel. First, the current-voltage curve was examined to see if ICP was occurring correctly (Figure 3) (Yang et al., 2015; Li et al., 2016) (Yang et al., 2015; Li et al., 2016). Then, we injected the sample of 700 μL into 3DP^2 with and without a pillar-structured channel. We applied the voltage (voltage step: 2 V) and measured the current with a current-voltage source measurement unit. In this graph, we observed three current regions: Ohmic, limiting, and over-limiting, with distinct characteristics. When a voltage was applied with a pillar-structured channel (red line), ions moved, and their speed (current) increased proportionally with the voltage in the ohmic region (<44 V). In the limiting region (44–86 V), the current could not be increased further when ion diffusion speed reached a certain level. However, in the case of permselective membranes (such as Nafion), there is one additional area. Over-limiting region (>86 V) appeared in permselective membranes, where vortices are created and supply ions to the limiting region. In this region, ICP phenomena occurred, and the depletion zone propagation started. The current response without a pillar-structured channel (gray line) was similar in the Ohmic region, but the current was not increased with high applied voltage (>44 V). We confirmed the ICP phenomenon with a current-voltage response. With structured pillar channels, we reduced the vortex and acquired more stability.

Preconcentration of color dye

To quantify the preconcentration performance of 3DP^2, we first tested the preconcentration of color and fluorescent dye with and without a pillar-structured channel (Figures 4, 5) under an applied voltage of 100 V. For the preconcentration operation, we injected a sample of 700 μL into 3DP^2 with and without a pillar-structured channel. The effect of the pillar-structured channel on depletion zone propagation was visually verified using the color dye (Orange-G). For the confirmation of ICP, we monitored the location of the depletion and enrichment zone in 3DP^2 every 5 min (Figure 4). Without a pillar-structured channel (Figure 4A), the depletion zone brittlely formed near reservoirs 4 to 5. The depletion zone was destroyed due to the vortex, so the depletion zone could not move toward reservoir 1 (anode side). The enrichment zone was difficult to find out the location. However, when we preconcentrated the sample with a pillar-structured channel (Figure 4B), the depletion zone stabilized and slowly moved to the anode side. In 20 min, the enrichment zone was formed in the reservoir 3. As seen in Figure 4B, we demonstrated the preconcentration of 3DP^2 using a large-volume color dye sample.

After preconcentration, we extracted 50 μL of preconcentrated sample from each reservoir to observe the preconcentration factor of each reservoir with a spectrophotometer (Nanodrop). In Figure 5, we compared the performance of preconcentration with (Figure 5B) and without (Figure 5A) a pillar-structured channel. First, we picked up the sample that was seen to be preconcentrated using a pipette. Furthermore, we analyzed the sample of preconcentration factor

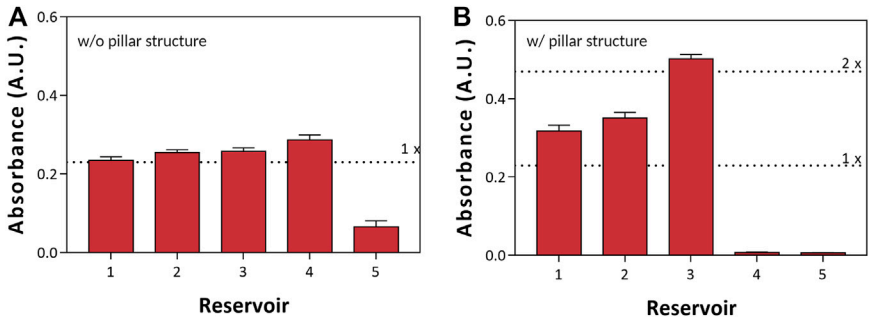

FIGURE 5
Preconcentration measurements of Orange-G with a spectrophotometer. **(A)** Without and **(B)** with a pillar-structured channel.

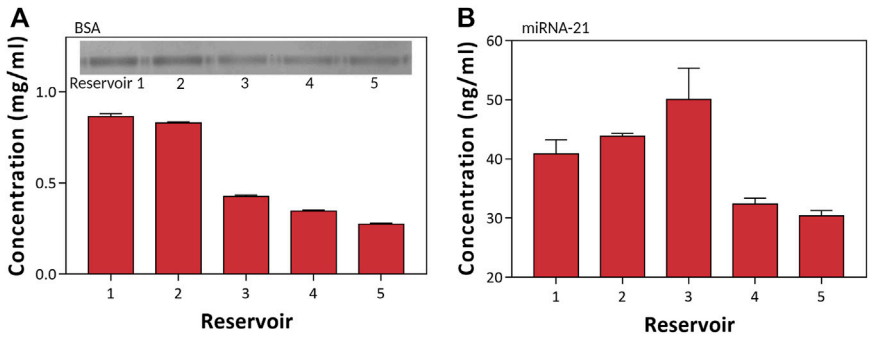

FIGURE 6
Preconcentration of BSA and miRNA-21. **(A)** Measurements of the BSA concentration of each reservoir using Nanodrop 280 nm wavelength and SDS-PAGE. **(B)** Measurements of the miRNA-21 concentration of each reservoir using Nanodrop 260 nm wavelength.

with a spectrophotometer. In the case without a pillar-structured channel (Figure 5A), reservoir five showed low absorbance according to the depletion zone; the absorbance of reservoir 4 was slightly higher than other reservoirs. On the other hand (Figure 5B), reservoirs 4 and 5 with a pillar-structured channels indicated low absorbance. Moreover, the enrichment zone was formed in reservoir three; the absorbance was high (preconcentration factor >2). We could easily pick up the preconcentrated sample with only a pipette and confirmed the effect and the preconcentration factor of a pillar-structured channels with fluorescent dye.

Demonstration of protein and miRNA preconcentration

To test the biomolecule preconcentration, we demonstrated the preconcentration of BSA, known as an inhibitor, and miRNA-21, known as a breast cancer biomarker (Wang et al., 2019; Zhang et al., 2016) (Zhang et al., 2016; Wang et al., 2019). For the preconcentration and separation of the sample, we first prepared BSA as a moderate molecule and miRNA-21 as a small molecule. Then, we prepared the mixture sample of BSA of 0.5 mg/ml and miRNA-21 of 30 ng/ml in 0.1 × PBS and injected it into the $3DP^2$ with and without a pillar-structured channel. We implemented the preconcentration of BSA and miRNA-21 with an applied voltage of 100 V. After the preconcentration, we extracted and analyzed each reservoir with a spectrophotometer (Figure 6). In Figure 6A, we observed the enrichment zone of BSA in reservoir 1 and reservoir 2. Moreover, we analyzed BSA concentration with SDS-PAGE in the inset photograph of Figure 6A. It also shows that reservoir 1 was a higher BSA concentration than the others (2-fold). In the case of miRNA-21, it was preconcentrated nearly two-fold in reservoir 3. As shown in Figure 5B, the small-size molecule was similarly preconcentrated in reservoir 3. Therefore, we could selectively separate by spatial in a target. The most concentrated location varied depending on the target because the point where electro-osmosis (Eq. 1) and electrophoresis (Eq. 2) achieved equilibrium was different depending on the size, charge, and buffer (Han

et al., 2019; Kwak et al., 2016) (Kwak et al., 2016b; Han et al., 2019). Therefore, the location of each material was different, and separation and concentration could be performed simultaneously.

$$\mu_{EOF} = \frac{\varepsilon\zeta}{4\pi\eta} \quad (1)$$

$$\mu_{EP} = \frac{q}{6\pi\eta r} \quad (2)$$

(ε: dielectric constant of the buffer, ζ: zeta potential of the device surface, η: buffer viscosity, q: charge of the biomolecule, r: radius of the biomolecule).

Conclusion

This work demonstrates that selective concentration is possible in large-capacity biomolecules. The conventional concentration methods using ICP enrich a small volume of samples and are difficult to extract, making downstream analysis challenging. A pillar-structured channel enriches many samples through vortex suppression, which can be easily picked-up from the reservoir, making it easy for downstream analysis with low cost (~$1.41). The pillar-structured channel electrically improves the ICP characteristics by I-V and I-t curves. Furthermore, the propagation of depletion is enhanced by suppressing the vortex through Orange-G. In addition, it was confirmed that biomolecules (BSA and miRNA-21) also can be concentrated and separated. The difference in concentration position based on the biomolecule properties is confirmed. With this study, we reveal that the separation of the material can be achieved by using the difference in the concentration position simultaneously with preconcentration. Further, we confirm that the ICP can be expanded to a large-capacity sample pretreatment. Therefore, this 3D reservoir-type ICP preconcentrator would provide a new strategy for downstream applications such as point-of-care diagnostics.

Data availability statement

The datasets presented in this article are not readily available because There is no restriction. Requests to access the datasets should be directed to yymsfam@naver.com.

Author contributions

Conceptualization, SL; Formal analysis, SL, JK, NL, and KK; Methodology, SP, JP, CK, and JH; Project administration, SL; Writing—original draft, SL; Writing—review and editing, SL, DY, YY, and JL. All authors have read and agreed to the published version of the manuscript.

Funding

This work was supported by the Bio & Medical Technology Development Program of the National Research Foundation funded by the Korean government (MSIT) (No. 2021M3E5E3080743). JL was supported by a research grant from Kwangwoon University in 2022.

Conflict of interest

The authors declare that the research was conducted in the absence of any commercial or financial relationships that could be construed as a potential conflict of interest.

Publisher's note

All claims expressed in this article are solely those of the authors and do not necessarily represent those of their affiliated organizations, or those of the publisher, the editors and the reviewers. Any product that may be evaluated in this article, or claim that may be made by its manufacturer, is not guaranteed or endorsed by the publisher.

References

Alele, N., and Ulbricht, M. (2016). Membrane-based purification of proteins from nanoparticle dispersions: Influences of membrane type and ultrafiltration conditions. *Sep. Purif. Technol.* 158, 171–182. doi:10.1016/j.seppur.2015.11.031

Anna, P. d., Jimenez-Martinez, J., Tabuteau, H., Turuban, R., Le Borgne, T., Derrien, M., et al. (2014). Mixing and reaction kinetics in porous media: An experimental pore scale quantification. *Environ. Sci. Technol.* 48, 508–516. doi:10.1021/es403105b

Bertrand, N., Wu, J., Xu, X., Kamaly, N., and Farokhzad, O. C. (2014). Cancer nanotechnology: The impact of passive and active targeting in the era of modern cancer biology. *Adv. Drug Deliv. Rev.* 66, 2–25. doi:10.1016/j.addr.2013.11.009

Brennan, K., Martin, K., FitzGerald, S. P., O'Sullivan, J., Wu, Y., Blanco, A., et al. (2020). A comparison of methods for the isolation and separation of extracellular vesicles from protein and lipid particles in human serum. *Sci. Rep.* 10, 1039. doi:10.1038/s41598-020-57497-7

Cao, Y., Chen, G., Wan, Y., and Luo, J. (2021). Nanofiltration membrane for bio-separation: Process-oriented materials innovation. *Eng. Life Sci.* 21, 405–416. doi:10.1002/elsc.202000100

Chen, D., Kim, J. T., Chamorro, L. P., and Timperman, A. T. (2021). Exceeding ohmic scaling by more than one order of magnitude with a 3D ion concentration polarization system. *Lab. Chip* 21, 3094–3104. doi:10.1039/D1LC00470K

Chen, J., Li, P., Zhang, T., Xu, Z., Huang, X., Wang, R., et al. (2021). Review on strategies and technologies for exosome isolation and purification. *Front. Bioeng. Biotechnol.* 9, 811971. doi:10.3389/fbioe.2021.811971

Deng, D., Dydek, E. V., Han, J. H., Schlumpberger, S., Mani, A., Zaltzman, B., et al. (2013). Overlimiting current and shock electrodialysis in porous media. *Langmuir* 29, 16167–16177. doi:10.1021/la4040547

Fan, J.-B., Luo, J., Luo, Z., Song, Y., Wang, Z., Meng, J., et al. (2019). Bioinspired microfluidic device by integrating a porous membrane and heterostructured nanoporous particles for biomolecule cleaning. *ACS Nano* 13, 8374–8381. doi:10.1021/acsnano.9b03918

Han, S. I., Hwang, K. S., Kwak, R., and Lee, J. H. (2016). Microfluidic paper-based biomolecule preconcentrator based on ion concentration polarization. *Lab. Chip* 16, 2219–2227. doi:10.1039/C6LC00499G

Han, S. I., Lee, D., Kim, H., Yoo, Y. K., Kim, C., Lee, J., et al. (2019). Electrokinetic size-based spatial separation of micro/nanospheres using paper-based 3D origami preconcentrator. *Anal. Chem.* 91, 10744–10749. doi:10.1021/acs.analchem.9b02201

Heikenfeld, J., Jajack, A., Feldman, B., Granger, S. W., Gaitonde, S., Begtrup, G., et al. (2019). Accessing analytes in biofluids for peripheral biochemical monitoring. *Nat. Biotechnol.* 37, 407–419. doi:10.1038/s41587-019-0040-3

Heitzer, E., Haque, I. S., Roberts, C. E. S., and Speicher, M. R. (2019). Current and future perspectives of liquid biopsies in genomics-driven oncology. *Nat. Rev. Genet.* 20, 71–88. doi:10.1038/s41576-018-0071-5

Hindson, C. M., Chevillet, J. R., Briggs, H. A., Gallichotte, E. N., Ruf, I. K., Hindson, B. J., et al. (2013). Absolute quantification by droplet digital PCR versus analog real-time PCR. *Nat. Methods* 10, 1003–1005. doi:10.1038/nmeth.2633

Kandlikar, S. G. (2008). Editor Dongqing Li (New York, NY, USA: Springer), 2093–2095.*Encyclopedia of microfluidics and nanofluidics*

Kim, C., Yoo, Y. K., Lee, N. E., Lee, J., Kim, K. H., Lee, S., et al. (2022). Nanoelectrokinetic-assisted lateral flow assay for COVID-19 antibody test. *Biosens. Bioelectron.* 212, 114385. doi:10.1016/j.bios.2022.114385

Kim, J., Cho, I., Lee, H., and Kim, S. J. (2017). Ion concentration polarization by bifurcated current path. *Sci. Rep.* 7, 5091. doi:10.1038/s41598-017-04646-0

Kim, K., Kim, W., Lee, H., and Kim, S. J. (2017). Stabilization of ion concentration polarization layer using micro fin structure for high-throughput applications. *Nanoscale* 9, 3466–3475. doi:10.1039/C6NR08978J

Kim, M., Jia, M., and Kim, T. (2013). Ion concentration polarization in a single and open microchannel induced by a surface-patterned perm-selective film. *Analyst* 138, 1370–1378. doi:10.1039/C2AN36346A

Kwak, R., Kang, J. Y., and Kim, T. S. (2016). Spatiotemporally defining biomolecule preconcentration by merging ion concentration polarization. *Anal. Chem.* 88, 988–996. doi:10.1021/acs.analchem.5b03855

Kwak, R., Pham, V. S., Kim, B., Chen, L., and Han, J. (2016). Enhanced salt removal by unipolar ion conduction in ion concentration polarization desalination. *Sci. Rep.* 6, 25349. doi:10.1038/srep25349

Lee, D., Lee, J. W., Kim, C., Chung, S., Yoon, D. S., et al. (2021). Highly efficient and scalable biomarker preconcentrator based on nanoelectrokinetics. *Biosens. Bioelectron. X.* 176, 112904. doi:10.1016/j.bios.2020.112904

Lee, H., Kim, J., Kim, H., Kim, H. Y., and Kim, S. J. (2017). A concentration-independent micro/nanofluidic active diode using an asymmetric ion concentration polarization layer. *Nanoscale* 9, 11871–11880. doi:10.1039/C7NR02075A

Li, M., and Anand, R. K. (2016). Recent advancements in ion concentration polarization. *Analyst* 141, 3496–3510. doi:10.1039/C6AN00194G

Li, M., and Anand, R. K. (2016). Recent advancements in ion concentration polarization. *Analyst* 141, 3496–3510. doi:10.1039/c6an00194g

Li, X., Niu, Y., Chen, Y., Wu, D., Yi, L., and Qiu, X. (2016). Microfluidic paper-based sample concentration using ion concentration polarization with smartphone detection. *Micromachines* 7, 199. doi:10.3390/mi7110199

Morini, G., et al. (2004). Laminar-to-turbulent flow transition in microchannels. *Microscale Thermophys. Eng.* 8, 15–30. doi:10.1080/10893950490272902

Nguyen, T. V., Gupta, R., Annas, D., Yoon, J., Kim, Y. J., Lee, G. H., et al. (2021). An integrated approach for the efficient extraction and solubilization of rice microsomal membrane proteins for high-throughput proteomics. *Front. Plant Sci.* 12, 723369. doi:10.3389/fpls.2021.723369

O'Connor, J. P., Aboagye, E. O., Adams, J. E., Aerts, H. J. W. L., Barrington, S. F., Beer, A. J., et al. (2017). Imaging biomarker roadmap for cancer studies. *Nat. Rev. Clin. Oncol.* 14, 169–186. doi:10.1038/nrclinonc.2016.162

Park, S., Jung, Y., Son, S. Y., Cho, I., Cho, Y., Lee, H., et al. (2016). Capillarity ion concentration polarization as spontaneous desalting mechanism. *Nat. Commun.* 7, 11223. doi:10.1038/ncomms11223

Prabhakar, P., Sen, R. K., Dwivedi, N., Khan, R., Solanki, P. R., Srivastava, A. K., et al. (2021). 3D-Printed microfluidics and potential biomedical applications. *Front. Nanotechnol.* 3. doi:10.3389/fnano.2021.609355

Purwidyantri, A., Domingues, T., Borme, J., Guerreiro, J. R., Ipatov, A., Abreu, C. M., et al. (2021). Influence of the electrolyte salt concentration on DNA detection with graphene transistors. *Biosensors* 11, 24. doi:10.3390/bios11010024

Razavi Bazaz, S., Rouhi, O., Raoufi, M. A., Ejeian, F., Asadnia, M., Jin, D., et al. (2020). 3D printing of inertial microfluidic devices. *Sci. Rep.* 10, 5929. doi:10.1038/s41598-020-62569-9

Sajid, M., Nazal, M. K., Mansha, M., Alsharaa, A., Jillani, S. M. S., and Basheer, C. (2016). Chemically modified electrodes for electrochemical detection of dopamine in the presence of uric acid and ascorbic acid: A review. *TrAC Trends Anal. Chem.* 76, 15–29. doi:10.1016/j.trac.2015.09.006

Tivey, A., Church, M., Rothwell, D., Dive, C., and Cook, N. (2022). Circulating tumour DNA — Looking beyond the blood. *Nat. Rev. Clin. Oncol.* 19, 600–612. doi:10.1038/s41571-022-00660-y

Wang, A., Wang, C., Tu, M., and Wong, D. (2016). Oral biofluid biomarker research: Current status and emerging Frontiers. *Diagnostics* 6, 45. doi:10.3390/diagnostics6040045

Wang, H., Tan, Z., Hu, H., Liu, H., Wu, T., Zheng, C., et al. (2019). microRNA-21 promotes breast cancer proliferation and metastasis by targeting LZTFL1. *BMC Cancer* 19, 738. doi:10.1186/s12885-019-5951-3

Yang, R.-J., Pu, H. H., and Wang, H. L. (2015). Ion concentration polarization on paper-based microfluidic devices and its application to preconcentrate dilute sample solutions. *Biomicrofluidics* 9, 014122. doi:10.1063/1.4913366

Zhang, C., Liu, K., Li, T., Fang, J., Ding, Y., Sun, L., et al. (2016). miR-21: A gene of dual regulation in breast cancer. *Int. J. Oncol.* 48, 161–172. doi:10.3892/ijo.2015.3232